Journal of Nuclear Materials 393 (2009) 433–448

Contents lists available at ScienceDirect

Journal of Nuclear Materials

journal homepage: www.elsevier.com/locate/jnucmat

High-temperature steam-oxidation behavior of Zr-1Nb cladding alloy E110

Y. Yan *, T.A. Burtseva, M.C. Billone

Nuclear Engineering Division, Argonne National Laboratory, Argonne, IL 60439, United States

ARTICLE INFO

Article history:
Received 18 December 2008
Accepted 24 June 2009

ABSTRACT

Oxidation experiments were conducted at 1000–1200 °C in flowing steam with samples of as-received Zr-1Nb alloy E110 tubing and/or polished E110 tubing. The purpose was to determine the oxidation behavior of this alloy under postulated loss-of-coolant accident conditions in light water reactors. The as-received E110 tubing exhibited a high degree of susceptibility to nodular oxidation and breakaway oxidation at relatively low test times, as compared to other cladding alloys. The nodules grew much more rapidly at 1000 °C than 1100 °C, as did the associated hydrogen uptake. The oxidation behavior was strongly affected by the surface condition of the materials. Polishing to ≈0.1 μm roughness (the roughness of the as-received tubing was ≈0.4 μm) delayed breakaway oxidation. Polishing also removed surface impurities. For polished samples oxidized at 1100 °C, no significant nodular oxidation appeared up to 1000 s. For polished samples oxidized at 1000 °C, hydrogen uptake >100 wppm was delayed from ≈300 s to >900 s. Weight-gain coefficients were determined for pre-breakaway oxidation of polished-only and machined-and-polished E110 tubing samples: 0.162 $(mg/cm^2)/s^{0.5}$ at 1000 °C and 0.613 $(mg/cm^2)/s^{0.5}$ at 1100 °C.

Published by Elsevier B.V.

1. Introduction

During a loss-of-coolant accident (LOCA) in a light water reactor (LWR), zirconium alloy cladding would be oxidized in high-temperature steam and would experience decreasing ductility with increasing oxidation level. The critical oxidation level at which the cladding embrittles is a function of oxidation temperature and hydrogen concentration. The LOCA is a major postulated accident considered in licensing and safety analyses. As such, extensive studies have been conducted over the past decades on the high-temperature steam-oxidation of fuel-rod cladding made of traditional zirconium alloys, such as Zircaloy-2 (Zry-2) and Zircaloy-4 (Zry-4) [1–9]. Advanced zirconium alloys, such as Zr–Sn–Nb and Zr-Nb, exhibit better corrosion resistance than Zry-4 under the operating conditions of pressurized water reactors (PWRs) [10–18]. Cladding alloys such as ZIRLO™ (Zr-1 wt.% Sn-1 wt.% Nb) and M5™ (Zr-1 wt.% Nb) have replaced Zry-4 in most US PWRs, and E110 (Zr-1 wt.% Nb) is used in PWRs designed by the Russian nuclear vender (TVEL).

A comparative study of the oxidation behavior of E110 and Zry-4 in the temperature range of 700–1100 °C. [19] showed remarkable differences between the two alloys with respect to morphology of the oxide and the oxygen-stabilized α-layer, hydrogen and oxygen pickup, and oxygen distribution in the metal. In addition, recent studies indicate dramatic differences in oxidation behavior between Zr-1Nb alloys M5 and E110 [10,14,18]. An extensive study of E110 was conducted at the Russian Research Center Kurchatov Institute and the Research Institute of Atomic Reactors [14], in which the following differences between Russian E110 and Western cladding alloys were considered and investigated: impurities in zircon ore, electrolytic refinement vs. Kroll process for reducing the ore to produce Zr for Zr-1Nb ingots, variations in alloying elements (e.g., oxygen), and differences in fabrication processes, especially surface finishing. Russian E110 alloys are fabricated from electrolytically refined Zr, while Western alloys such as M5 are fabricated by the Kroll process from sponge Zr. The Russian results [14] suggest that electrolytic refinement removes impurities, may help stabilize the oxide layer grown on the cladding surface. Ref. [14] also reports the positive effect of surface polishing on delaying breakaway oxidation time. These tests were conducted after Argonne had completed its study of polished-only and machined-and-polished E110 tubing samples.

Since the mid-1990s, the US Nuclear Regulatory Commission (NRC) has sponsored a cooperative research program at Argonne National Laboratory (ANL) to address the effects of fuel burnup on the embrittlement of various cladding alloys subjected to laboratory tests relevant to LOCA conditions. The advantage of this approach is that the behavior of cladding alloys tested under the same conditions can be compared directly. In reviewing data from other laboratories [20–24], we had difficulty in comparing the behavior of different cladding materials, because of differences in heats and surface finish of materials, sample preparation techniques, and heating–cooling methods. The ANL results are documented in NUREG/CR-6967 [18]. Although Russian E110 is not used in US reactors, we conducted a series of two-sided

* Corresponding author. Tel.: +1 630 252 9560; fax: +1 630 252 2785.
E-mail address: yan@anl.gov (Y. Yan).

0022-3115/$ - see front matter Published by Elsevier B.V.
doi:10.1016/j.jnucmat.2009.06.029

steam-oxidation tests with as-received E110 and modified E110 tubing samples at high-temperature (1000–1200 °C) for the purpose of gaining better understanding as to why this particular Zr-1Nb alloy experiences such early breakaway oxidation and ductility loss for these steam-oxidation temperatures.

Zirconium dioxide can exist in several crystallographic forms. The normal tetragonal oxide that develops under LOCA conditions at $\geqslant$1000 °C is dense, strong, adherent, and protective with respect to hydrogen pickup. Although the nominal monoclinic-to-tetragonal phase change temperature is $\approx$1150 °C for stress-free stoichiometric ZrO_2, the tetragonal phase can be stabilized at lower temperatures, as low as room temperature (RT) for partially stabilized zirconia, as a result of hypostoichiometry [$ZrO_{(2-x)}$], impurities (e.g., Ca and Mg), and compressive stress. The outer-surface of this oxide has a lustrous black appearance at RT. There are, however, conditions that promote a transformation to the monoclinic phase – the phase that is grown during normal operation – that is neither strong, nor fully dense, nor fully protective with respect to hydrogen pickup, except for thin oxides grown during relatively low burnup. According to Leistikow and Schanz [3,4], the tetragonal-to-monoclinic transformation observed at <1050 °C on Zry-4 is an instability that initiates at local regions of the scalloped metal-oxide interface due to stress reversals and grows rapidly throughout the oxide layer. However, certain chemical impurities (e.g., F) on the surface or in the substrate can induce early transformation, which does not necessarily initiate at the metal-oxide interface. The outer-surface of monoclinic oxide formed at high-temperature is gray for Zircaloy, yellow for ZIRLO, and grayish-white for E110. As this transformation results in an increase in oxidation rate, it is referred to as "breakaway oxidation." Along with this increase in oxidation rate due to cracks in the monoclinic oxide, there is significant hydrogen pickup. Hydrogen that enters in this manner during a LOCA transient has an embrittlement effect similar to the hydrogen picked up by the cladding during normal reactor operating conditions. Breakaway oxidation times reported in the literature for E110 are as low as 500 s based on ductility loss, >200-wppm hydrogen pickup, weight-gain-rate increase, and/or visual appearance. However, in reviewing the literature for E110, we found that other labs used E110 samples from heats different from the ones used at ANL. Comparison of the data sets was difficult because oxidation test methods varied considerably (e.g., heating and cooling rates), as did E110 chemistry, thermomechanical treatment, and surface finish.

Argonne modifications to as-received E110 samples included polishing alone, as well as machining and polishing (M–P). Also performed for comparison were one-sided tests at 1100 °C with as-received E110. These tests were designed to isolate material factors (surface roughness, surface chemistry, substrate chemistry and microstructure, and bulk chemistry and microstructure) that may be responsible for the formation of monoclinic oxide and the early breakaway oxidation times. Ring compression tests were performed on selected E110 specimens to determine their ductility, which decreased significantly with the appearance of nodular oxide formation and breakaway on the sample surface. Hydrogen pickup during high-temperature steam-oxidation was measured for specimens that had surface regions of white nodular oxide, resulting in high hydrogen pickup, and uniform black oxide, resulting in low hydrogen pickup. Crystallographic analyses were not performed in this study to confirm the presence of tetragonal, mixed tetragonal-monoclinic, or monoclinic oxide phases. Rather, the oxide phases were determined by their physical appearance, morphology and behavior with respect to hydrogen pickup and the growth rate of the oxide layer thickness. Using the ANL furnace's viewing port, we observed outer-surface color changes associated with breakaway oxidation during high-temperature oxidation rather than during the cooling phase.

2. Sample preparation and experimental procedure

The test material was as-received E110 tubing and cladding (supplied by the Finnish company, Fortum). Two kinds of samples were received for this study: 1) cladding that was the finished product (i.e., pickled and anodized) and 2) tubing that was in the E110 condition prior to the anodizing used to increase surface hardness. The results described in this report are from tests conducted with tubing characterized by an outer diameter of 9.17 mm, a wall thickness of 0.71 mm, and a root-mean-square surface roughness of 0.35 μm. The hydrogen concentration for this as-received tubing was <10 wppm.

Table 1 lists the measured concentrations of major alloying elements and some impurities in E110 used in the ANL study, along with the E110 specifications reported by Shebaldov et al. [12]. Although Fe, Sn and C concentrations are higher than "typical" values, while Hf is lower than the typical value, the chemistry of the Fortum-supplied E110 is essentially within E110 specifications.

In addition to the as-received tubing tested, sets of E110 tubing samples were prepared by polishing or machining and polishing the cladding surfaces to investigate separate effects: outer-surface polishing only, outer-surface M–P only, outer- and inner-surface polishing, and outer-surface polishing with inner-surface M–P. For as-received and machined samples, surface polishing was performed with 9-μm-grain Al_2O_3 paper for 2 min, followed by 3-μm-grain diamond paper for 3 min. The machine-removed thickness varied from 20 to 110 μm. Polishing resulted in the removal of a few microns and in a surface roughness of 0.14 μm.

Transmission electron microscopy (TEM) examinations of the as-received E110 were carried out with a Philips CM-30 microscope operated at 200 kV. The specimens were prepared in the plane view of the cladding surface; the electron beam of the microscope was perpendicular to the surface. The TEM specimen was a thin foil of the tubing, which was $\approx$3 mm in diameter, and the areas observed were approximately 0.5 × 0.5 μm. The TEM results were supplemented by scanning electron microscopy (SEM) and energy dispersive X-ray spectroscopy (EDX) analyses.

The 25-mm-long samples were cut from E110 tubing for oxidation tests. Before these tests, the diameter of each sample was measured with a micrometer to an accuracy of ±0.025 mm at

Table 1
Chemical composition of E110 used in oxidation studies.

Element	E110 specification (typical values)[a]	Fortum E110 measured by CONAM[b]	Fortum E110 measured by ANL[b]
Zr, wt.%	Balance	Balance	Balance
Nb, wt.%	0.9–1.1 (0.95–1.10)	1.03	–
O, wppm	⩽1000 (500–700)	500	505
Fe, wppm	⩽500 (140)	550 ± 150	–
Cr, wppm	⩽200 (<30)	<100	–
Sn, wppm	⩽500 (<100)	200	–
Ni, wppm	⩽200 (<30–39)	<100	–
S, wppm	–	25 ± 15	–
C, wppm	⩽200 (<40–70)	135	–
Hf, wppm	⩽500 (300–400)	100	–
Si, wppm	⩽200 (46–90)	100	–
N, wppm	⩽60 (<30–40)	46	–
H, wppm	⩽15 (4–7)	5	5
Ca, wppm	⩽300 (<100)	–	–
K, wppm	⩽40 (<30)	–	–
F, wppm	⩽30 (<30)	–	–
Cl, wppm	⩽30 (<7)	–	–
Al, wppm	⩽80 (<30)	–	–

[a] Shebaldov et al. [12].
[b] Chemical data provided by CONAM Materials Analysis Group; H and O content confirmed by Argonne National Laboratory (ANL).

two azimuthal orientations 90° apart at the axial center of the sample. Length measurements were also taken. The sample was first cleaned with ethanol and then in distilled water in an ultrasonic bath for ≈200 s. Sample weights were measured before and after each test with a balance to an accuracy of ±0.0001 g.

The experimental arrangement used to oxidize E110 in steam, as shown in Fig. 1, consists of a radiant furnace, pressure system to internally pressurize/purge the 25-mm-long test sample for one-sided oxidation tests, steam supply system, quench system, and test train. The furnace is a quad-elliptic, focused radiant heater with a 250-mm-long heating zone. With the test train and sample positioned within the furnace, the uniform temperature zone is ⩾100 mm. The furnace is centered with respect to a quartz tube, which contains the test train and the flowing steam. The test train, which holds the sample, is centered relative to the quartz tube by perforated spacer discs. Tests were conducted with average steam flow rates of ≈0.32 ± 0.03 g/(cm^2/min) (deduced from water consumption), a rate at which the oxidation rate is independent of the steam flow rate [8]. The system is designed to perform both one-sided (outer-surface) and two-sided oxidation tests.

Steam flows from the bottom through the quartz tube and along the outer-surface of the sample for the one-sided tests. Alumina inserts prevent direct contact between the Inconel holder and the Zr-based alloy sample. For the two-sided oxidation tests, the test train has six or eight holes in the Inconel holder just below (three or four holes) and above (three or four holes) the sample for steam flows to the inner-surface. The main objectives in designing the two-sided oxidation tests were to ensure adequate steam flow inside the sample and to demonstrate accurate temperature monitoring and control. The criteria adopted for ensuring adequate steam flow were: low hydrogen pickup for temperature–time regimes consistent with CINOG results [25] for M5 alloy and oxide layer thickness on the inner-surface approximately equal to that on the outer-surface. Weight-gain was also a criterion used, but it proved to be relatively insensitive to the design improvements. Extensive temperature benchmarking tests were performed to ensure minimum temperature overshoot of the sample during heating and to correlate the sample temperature rise with that of the control thermocouple and the other two thermocouples located on the Inconel holder just above the sample (120° apart).

Thermal-benchmark Test EU#9 had two thermocouples (TCs) welded directly onto the outer-surface of the sample. Its temperature history is given in Figure 85 of Ref. [18]. Unlike the other alloys tested, significant buildup of gray monoclinic oxide occurred around the TCs welded to the E110 sample. For the one-sided oxidation tests at 1100 °C, an argon purge (at higher pressure than the steam) flowed through the center of the sample to further minimize inner-surface oxidation. Based on detailed analyses of the test results, inner-surface oxidation occurred only near the ends of the sample, leaving the middle 80% of the sample inner-surface free from oxidation. Three TCs were welded 120° apart on the Inconel holder just above the sample. A fourth TC was suspended within the sample at the midplane, which was used for data analysis. Based on benchmark tests with TCs welded to the sample outer diameter (OD), the suspended TC reading was in excellent agreement with the average of the sample OD readings [6]. For the long hold times used in our tests, the difference in weight-gain calculated by the Cathcart-Pawel (CP) model [2] was ⩽5% between the sample temperature history and the internal TC history.

For 8-mm-long samples sectioned from samples exposed to two-sided oxidation at 1000 °C, ring compression tests were performed at room temperature or 135 °C and a displacement rate of 0.0333 mm/s in a Table Mounted Materials Testing System (Instron Model 5566). The load–displacement curves were analyzed in the standard way: linearize the initial loading curve, use the

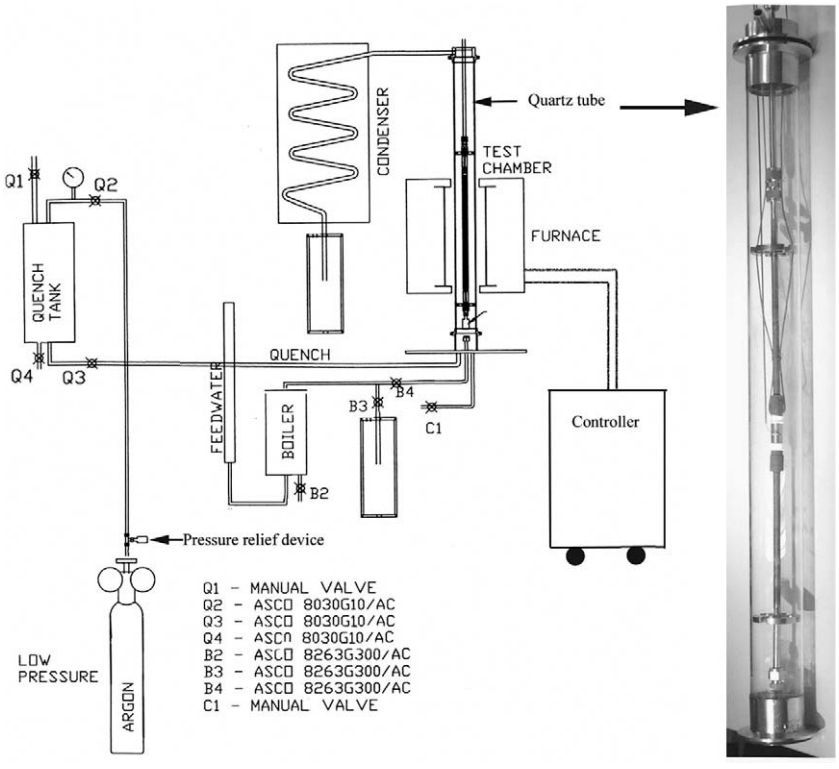

Fig. 1. Schematic illustration of the oxidation system and the oxidation test train assembly.

slope of the initial loading curve to mathematically "unload" the sample at the peak load before a significant load drop (≈30–50%) indicating a through-wall crack along the length of the sample, and determine the offset displacement (distance along the displacement axis between loading and unloading lines). The permanent displacement is determined directly by measuring the pre-test and post-test diameter in the loading direction. For all tests in which both offset and permanent strains could be compared, the more accurate permanent strain was less (0–2% strain) than the offset strain. The offset and permanent displacements were normalized to the pre-oxidation test sample OD to determine the relative plastic strain.

3. Results

3.1. Pre-test characterization of E110 cladding

Fig. 2a–d shows micrographs of the as-received E110 outer-surface. At lower magnification, both axial and circumferential striations and grooves – deeper than the random roughness – are evident. At higher magnifications, the circumferential grooves, as well as the defects between the grooves, are apparent. SEM/EDX was used to examine the chemical composition in the defect areas; no impurities could be detected, possibly due to the limited resolution of the SEM. Fig. 2e–h shows the outer-surface after

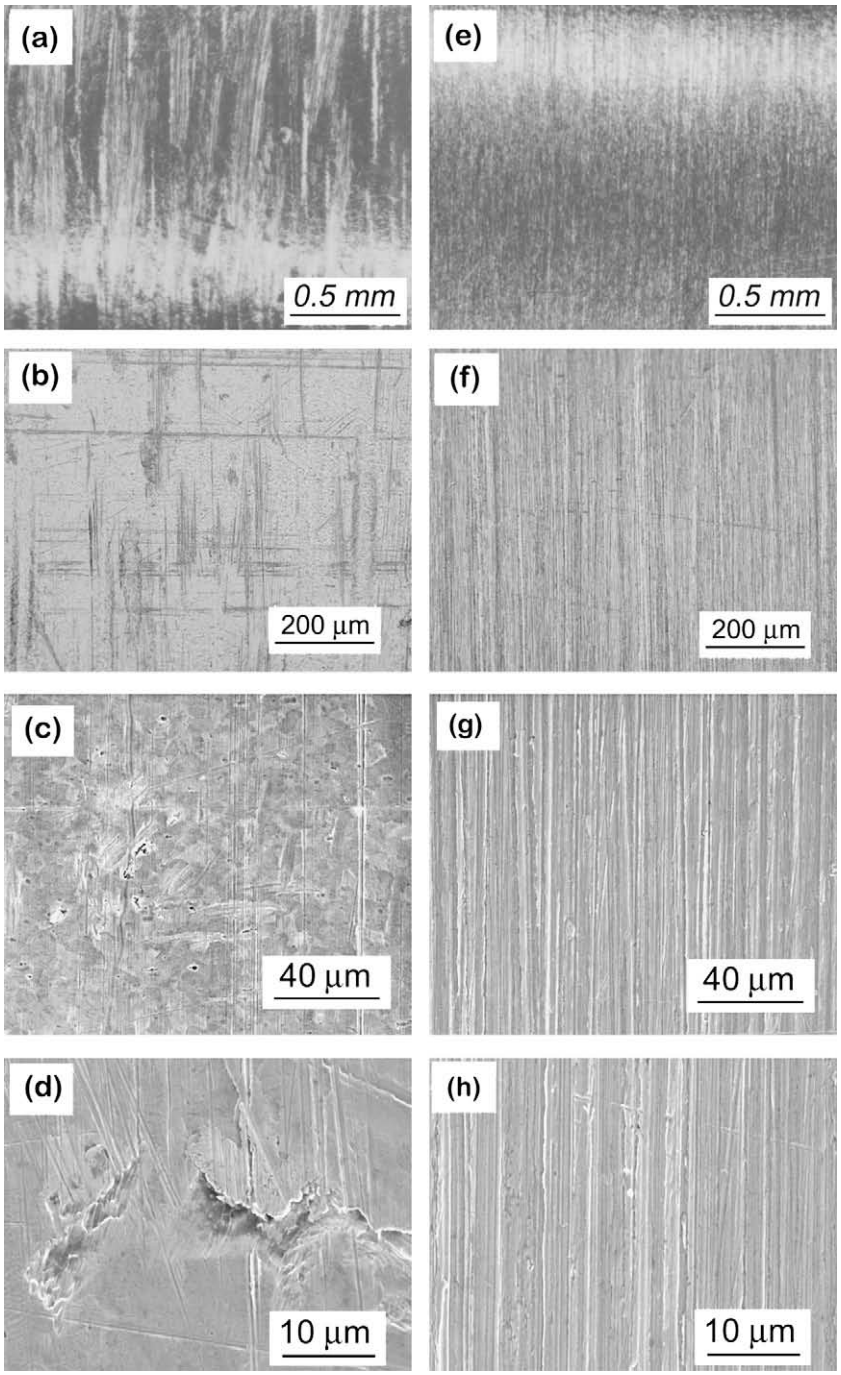

Fig. 2. The outer-surface of as-received E110 tubing (a–d) with measured surface roughness of 0.35 μm and polished E110 (e–h) with measured surface roughness of 0.13 μm. Vertical direction in micrographs corresponds to the circumferential direction of the tubing.

machining and polishing. The rough surface is smoothed out by the polishing. No defects at sizes comparable to those for the as-received sample (Fig. 2d) were observed for the polished sample (Fig. 2h).

Our SEM and TEM studies of as-received E110 indicate that the observed area is a mixture of grains, whose sizes vary from 1 to 13 μm (see Fig. 3a). The grains are mostly equiaxed, as shown in Fig. 3b. The average grain size was determined to be ≈4.5 μm. No obvious grain elongation was observed in the longitudinal direction. Fig. 3c shows the grain size distribution. Some secondary phase particles (SPP) appeared within the grains. However, they were difficult to analyze due to the limited spatial resolution of SEM. Fig. 4a is a low-magnification TEM micrograph showing precipitates inside of grains for as-received E110 tubing. Detailed examinations at higher magnification show different shapes of precipitates and the related strain field contrast. To minimize dynamical diffraction contrast effects, we used a tilted view with the bright field under the weak diffraction condition. In this way, the precipitates can be observed more clearly. The precipitates appear to consist of a mixture of small particles (<50 nm) and large particles (100–250 nm), as shown in Fig. 4b. A nonuniform cluster of precipitates appeared in some local areas (Fig. 4c), while the precipitates documented for M5 [10] were evenly distributed. If clusters of Nb-rich precipitates characterize the bulk of the material, such precipitates could negatively impact the steam-oxidation behavior of E110. However, more regions of E110 would have to be examined to determine if such clusters are rare or characteristic of the material.

Fig. 5 shows the results from EDX analyses for the E110 matrix and the small and large precipitates labeled as such in Fig. 4b. Fig. 5b indicates that the small precipitates are Nb-rich. The larger precipitates contain less Nb, but some Fe (Fig. 5c). The large precipitates are Laves-phases [$Zr(Nb,Fe)_2$], while small precipitates are likely beta-Nb phases. Most of the observed precipitates are round; however, some precipitates having faceted surfaces were observed at a grain boundary in E110. Shishov et al. [26] and Yegorova et al. [14] examined the SPP in E110 by means of TEM/EDX and observed

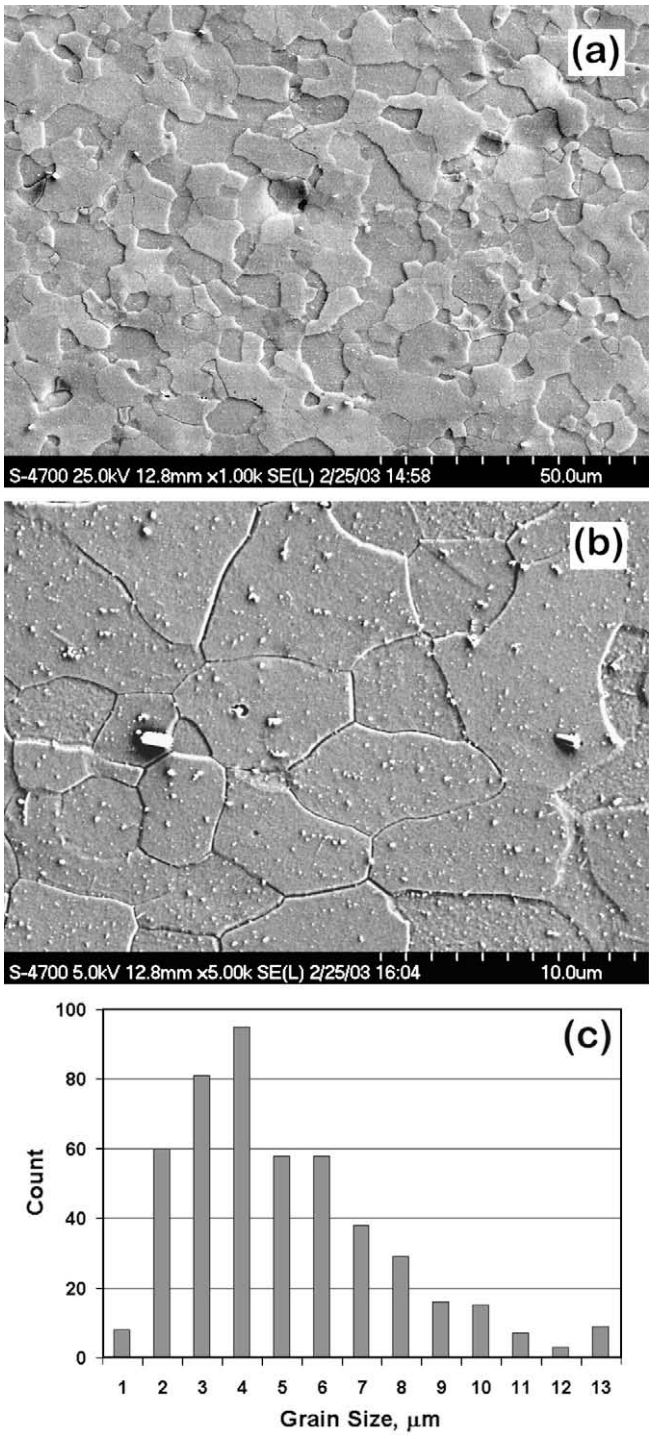

Fig. 3. (a) SEM micrograph, (b) higher magnification micrograph, and (c) grain size distribution in as-received E110 tubing.

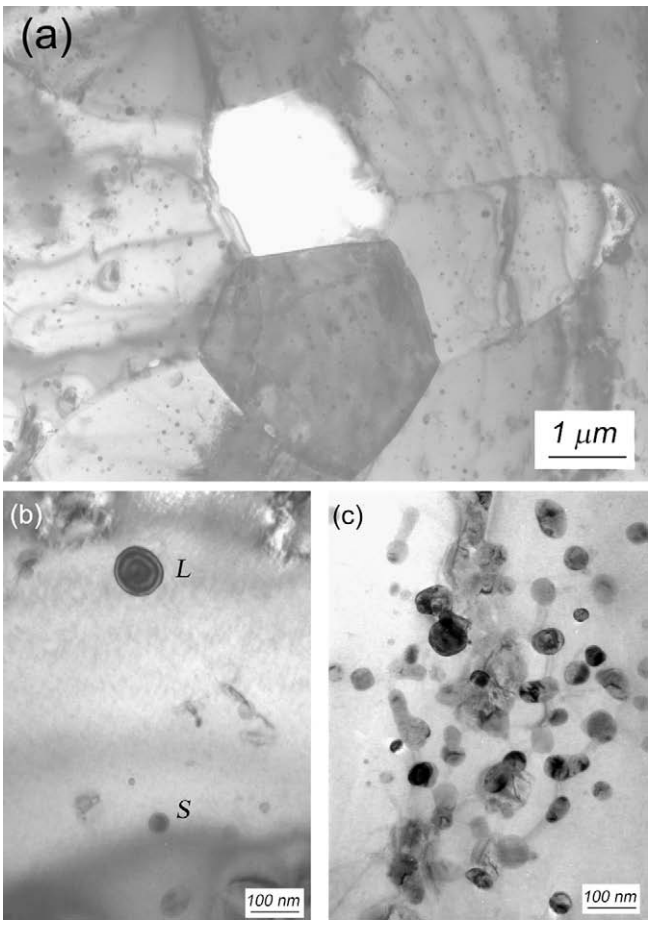

Fig. 4. TEM micrographs of as-received E110 tubing showing (a) grains and precipitates inside the grains, (b) a large (L) precipitate (size of ≈105 nm) and a small (S) precipitate (size of ≈45 nm), and (c) high density of precipitates in a local area.

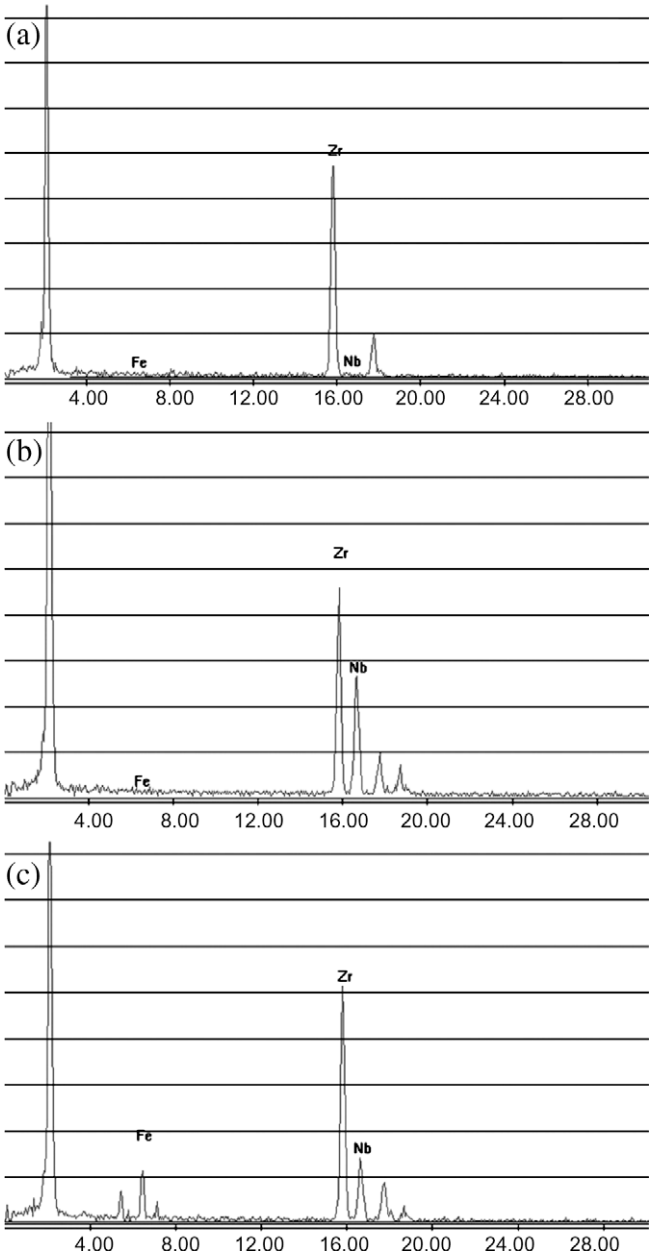

Fig. 5. Energy dispersive spectra obtained from (a) E110 matrix, (b) the small precipitate in Fig. 4b (labeled as S), and (c). The large precipitate in Fig. 4b (labeled ads L). Larger precipitates typically contain less Nb, but some Fe.

only beta-phase particles enriched with niobium. Our TEM examinations also revealed some structural defects in as-received E110, but no impurity could be detected by EDX analyses.

3.2. Two-sided steam-oxidation of as-received E110 at 1000 °C

Two-sided steam-oxidation tests were conducted with as-received E110 tubing samples to determine the effects of time at 1000 °C on the uniformity of the oxide layer and on the hydrogen pickup. The results are summarized in Table 2. For test planning purposes, the CP correlation, which is based on data for Zry-4 [2], was used to calculate the normalized weight-gain due to oxygen pickup and the corresponding equivalent cladding reacted (ECR). Note that some advanced alloys, such as M5, exhibit significantly lower weight-gain than that of Zry-4 and the CP-predicted weight-gain at 1000 °C. Some previous data have also shown oxidation kinetics more or less cubic under such conditions for Nb-containing alloys with compositions similar to those for ZIRLO [20] and M5 [22]. Because of the relatively early nodular breakaway oxidation and the resulting nonuniformity of the oxide layer, no attempts were made to determine the "experimental" ECR based on the measured weight-gain or the Zr consumed. Although pre- and post-test sample weights were recorded, the more brittle white regions tended to partially flake off during the test, especially during the cooling phase and during post-test handling, thus rendering the measurement of post-test sample weight as unreliable. Caution should thus be exercised in comparing the CP-calculated ECR values listed with those determined experimentally or by other correlations.

For the CP correlation developed for Zry-4, Δw_o = normalized weight-gain in mg/cm^2, t = time in seconds, and k = the weight-gain coefficient for isothermal oxidation. For parabolic kinetics associated with the formation of a protective black tetragonal oxide, the CP equation for isothermal exposure to steam at 1000–1200 °C is

$$\Delta w_o = k \cdot t^{0.5} \tag{1}$$

and the corresponding ECR (%) for the E110 geometry and two-sided oxidation [2] is

$$\mathrm{ECR} = 1.235\,\Delta w_o \tag{2}$$

Consistent with the oxidation kinetics reported in Ref. [2] and with what most researchers report as the CP correlation, $k = 0.2242$ (mg/cm^2)/s$^{0.5}$ is used to determine the predicted weight-gain and ECR at 1000 °C. Note that the CP-calculated values for Δw_o and ECR listed in Tables 2–4 are determined by integrating the rate form of Eq. (1) over the temperature history determined from thermal benchmark tests with TCs welded directly onto the sample. All of the calculated results in Table 2 are based on integration of the average of the temperature histories for the two benchmark TCs. The ramp time from 300 °C to 1000 °C was about 75 s, with most of that time spent at 900–1000 °C. However, a higher ramp rate was used for the EU#8 test sample.

Shown in Fig. 6 is the E110 surface oxidized in steam at 950–1000 °C for hold times of 5–1400 s. After the 75-s ramp and the 5-s hold time, the oxide layer on the EU#10 sample appears to be lustrous black and uniform (Fig. 6a). However, high-magnification images (Fig. 7) reveal the presence of "white spots" in the black matrix. We assume that these are initiation sites for nodular oxidation, for which the behavior is consistent with that of the weaker monoclinic-oxide phase.

Test EU#12 was run for 290 s at 1000 °C. It developed local regions of nodular oxidation as well as interconnected regions (Fig. 6b). Local delamination of the oxide was found essentially down to the base metal. This result is consistent with the measured hydrogen concentration (120 ± 45 wppm) of the sample. A test was run at 950 °C for the same 290-s hold time. Based on calculation models, both the weight-gain and ECR should have been smaller for this sample than for the sample tested at 1000 °C. However, the extent of monoclinic oxide formation and cracking appears similar to, or even greater than, that for the sample tested at 1000 °C. Complete delamination and spallation are shown in Fig. 6d for the EU#8 sample tested for 1400 s at 1000 °C. As the measured hydrogen uptake for EU#8 (≈4200 wppm) was well beyond the amount needed for E110 embrittlement, test times between 290 s and 1400 s were explored to map the evolution of hydrogen uptake with time and calculated ECR. Extensive hydrogen measurements were performed to determine the axial and circumferential variation of hydrogen uptake with time. We found that hydrogen uptake

Table 2
Two-sided steam-oxidation tests conducted at 1000 °C with as-received E110 cladding samples (9.17-mm outer diameter [OD], 0.71-mm wall thickness, and 0.35-μm OD surface roughness). Ring compression tests were performed on 8-mm-long samples at room temperature (RT) and at cross-head displacement rate of 2 mm/min.

Test ID#	t_s[a] (s)	Pred. ECR (%)	Pred. Δw_p[b] (mg/cm^2)	Measured ECR (%)	H content[c] (wppm)	RT Offset displacement (mm)	RT ductility (%)	Sample condition observations
E110	0	0	0	–	3	6	66	
EU#10	5	1.8	1.49	$\geqslant$1.3	–	6.05	66	Uniform black oxide layer; white spots $\leqslant$ 50 μm
EU#9	290	5.0	4.07	>3.7	–	–	–	Extensive monoclinic oxide around welded TCs
EU#12	290	5.0	4.07	>3.3	120 (70–170)	5.44	59	Nonuniform oxide
EU#11	290 at 950 °C	<5	<4	–	–	–	–	Oxide surface appears worse than EU#12 sample
EU#36	395	5.8	4.67	>3.8	32 (4–84)	5.82	63	Nonuniform oxide layer
EU#38	625	7.1	5.78	>5.6	275 (25–560)	0.13	1.4 (brittle)	Axial distribution of hydrogen content
EU#38A	625	7.1	5.78	–	≈125 ≈(25–285)	–	–	Axial distribution of hydrogen content
EU#40	825	8.1	6.59	>5.8	925 (440–1500)	0.04	0.4 (brittle)	Delamination–spallation from half the sample
EU#8	1400	10.4	8.39	–	4230 ± 250	0	0	Extensive delamination–spallation

[a] t_s = hold time at 1000 °C; ramp from 300 °C to 1000 °C: 75 s.
[b] Δw_p = CP-model-predicted normalized weight-gain, which was developed for Zry-4. The correlation gives higher-than-measured values for Zr-1Nb alloys prior to breakaway oxidation at 1000 °C.
[c] Numbers in parentheses show range.

Table 3
One-sided steam-oxidation tests at 1100 °C for as-received E110.

Test ID	Hold time (s)	Pred. ECR (%)	Pred. Δw_o[a] (mg/cm^2)	Meas. Δw_o[b] (mg/cm^2)	H content (wppm)	Comment
EU#3	200	3.6	5.6	5.3	–	White spots observed at high mag.
EU#2	512	5.8	9.0	9.0	–	Visible white spots
EU#2A[c]	512	5.8	9.0	8.2	–	Visible white spots (anodized sample)
EU#1	1400	9.6	14.9	14.1	–	Visible white spots
EU#4	2473	11.8	18.3	24.0	182	Regions of cracked white oxide, and pronounced nodes
EU#5	3800	15.8	24.6	37.5	204	Larger regions of cracked white oxide

[a] Δw_o is the surface-area-normalized weight-gain due to oxygen pickup.
[b] Measured weight-gains are not reliable because of partial inner-surface oxidation near sample ends and flaking off of monoclinic oxide from the outer-surface.
[c] Test EU#2A was conducted with an etched-and-anodized cladding sample.

Table 4
Two-sided oxidation tests with modified E110 cladding at 1000 °C. Polished cladding outer diameter is 9.17 mm, machined-and-polished inner diameter is 7.98 mm, and wall thickness is 0.6 mm.

Test ID#	t_s[a] (s)	Pred. ECR (%)	Pred. Δw_p[b] (mg/cm^2)	Meas. Δw_m[c] (mg/cm^2)	H content (wppm)	Outer-surface oxide
EU#25	0	1.8	1.5	1.5	–	Lustrous black
EU#19	41	2.6	2.1	1.9	–	Lustrous black
EU#20	106	3.3	2.7	2.3	–	Lustrous black
EU#21	190	4.2	3.4	2.7	–	Lustrous black
EU#22	292	5.2	4.2	3.1	–	Lustrous black
EU#23	413	5.9	4.8	>3.4	–	Lustrous black with white spots at 236 s
EU#24	413	5.9	4.8	>3.1	11 ± 5	Lustrous black with white spots at 281 s
EU#26	413	5.9	4.8	>2.9	–	Lustrous black with white end regions
EU#27	413	5.9	4.8	>3.0	–	Lustrous black with white end regions
EU#37	815	8.1	6.6	–	6 ± 1	–
EU#16	1025	9.1	7.4	–	150 (32–342)	See Fig. 14 for variation in outer-surface oxide layer
EU#41	2025	12.5	10.1	–	1280 ± 100	–

[a] t_s = time at the sample hold temperature.
[b] Δw_p = predicted normalized weight-gain based on CP correlation.
[c] Δw_m = measured normalized weight-gain based on sample weight change; ECR = 1.235 Δw is referenced to the as-received E110 wall thickness of 0.71 mm.

was locally high under regions of cracked white oxide and locally low under regions of uniform black oxide. This difference led to significant circumferential and axial variations in hydrogen content. The results in Table 2 represent circumferentially averaged values, which are used for correlation with ring compression test results. Large circumferential and axial variations in hydrogen are expected during the breakaway oxidation phase. Hydrogen pickup is highly localized and concentration-driven diffusion is time dependent. At longer oxidation times, well beyond the point of embrittlement, the hydrogen concentration becomes more uniform. Also, it should be realized that no two samples are identical with respect to scratches, roughness and

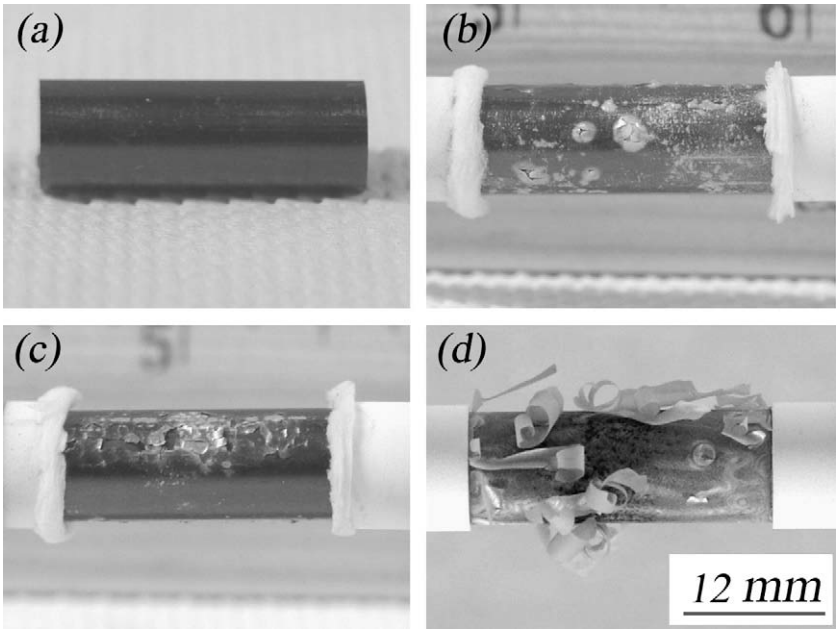

Fig. 6. Appearance of as-received E110 outer-surface after steam-oxidation for (a) 5-s hold time at 1000 °C, (b) 290-s hold time at 1000 °C, (c) 290-s hold time at 950 °C, and (d) 1400-s hold time at 1000 °C.

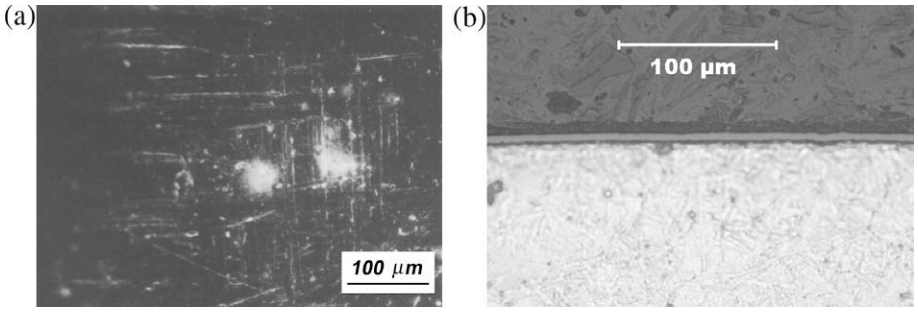

Fig. 7. (a) Plane-view micrograph showing initiation of sites for nodular monoclinic oxide growth on as-received E110 tubing surface and (b) cross-sectional view of a flat interface between the oxide and metal layers. The sample was heated from 300 °C to 1000 °C in 75 s and held at 1000 °C for 5 s prior to cooling.

chemical impurities. Thus, considerable scatter in results for hydrogen pickup vs. time may occur due to an instability phenomenon such as breakaway oxidation.

The hydrogen measurements for the two-sided oxidation samples at 1000 °C are summarized in Fig. 8, where hydrogen-content is plotted vs. CP-predicted ECR. On the basis of the central location values from which ring compression samples were cut, embrittlement is expected to occur in the range of 300–600 s, with corresponding CP-predicted ECR values of ≈5–7%. Because of the observed end effects, samples >25 mm may have a somewhat longer transition time and higher ECR than the 25-mm-long samples tested in this program. However, our results are generally consistent with the results for the 100-mm-long samples tested by Yegorova et al. [14]. Results shown in Fig. 8 for ANL-polished samples and KFKI samples are discussed in Section 3.4.1.

We conducted a limited number of ring-compression tests at room temperature in an effort to correlate ductility decrease with hydrogen pickup. As these samples experienced significant breakaway oxidation, partial-to-full delamination of the oxide layer, and partial spallation of the oxide layer, the measured change in sample weight represents a lower bound on the degree of oxidation.

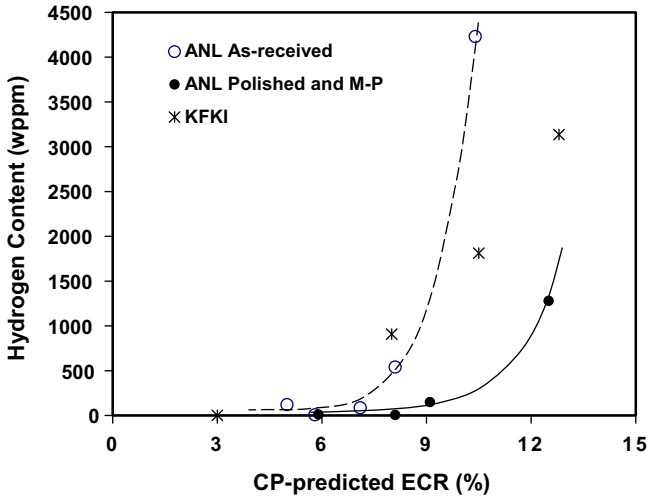

Fig. 8. Hydrogen content vs. CP-predicted ECR of tubing samples after two-sided oxidation tests at 1000 °C for as-received E110 tubing tested at ANL, for polished E110 tested at ANL, and for E110 tested at KFKI [24].

The results for hydrogen pickup and post-oxidation ductility for as-received E110 samples oxidized at 1000 °C and furnace cooled are summarized in Table 2. For hold times at 1000 °C between ≈300 s and ≈600 s, there was a transition between ductile and brittle behavior. Samples with <2% offset strain are assumed to be brittle. The oxide layer had already experienced local breakaway oxidation by ≈300 s, resulting in an average hydrogen pickup of 120 wppm. By ≈600 s hold time, the extent of the sample surface experiencing breakaway oxidation increased, resulting in local variation in hydrogen pickup from 25 to 560 wppm. The average value for the sample tested at ≈600 s hold time was 275 wppm. However, the critical hydrogen level for embrittlement of E110 at 1000 °C could not be determined precisely from the data in Table 2 because of the wide variation in hydrogen content within a single sample. As shown in Fig. 9a, E110 appears to lose its RT ductility with hydrogen pickup in the range of 120 to 275 wppm. The corresponding calculated ECR for embrittlement is ≈7% at 1000 °C, as shown in Fig. 9b.

3.3. One-sided steam-oxidation of as-received E110 at 1100°C

Oxidation tests were conducted at 1100 °C to investigate the evolution of the breakaway oxidation and embrittlement observed by other investigators [14,19]. In our study, high ramp rates were used for these tests, so that the hold time at 1100 °C essentially represented the total time from ramp initiation at 300 °C to test completion at 1100 °C. Table 3 summarizes test conditions and results for these tests.

Shown in Fig. 10 is the E110 surface oxidized in steam at 1100 °C for test times of 100 s to 3800 s. Although nodular oxidation occurred at 1100 °C, the nodules were much more localized than they were at 1000 °C for comparable test times. Metallographic examinations indicated that local breakaway oxidation had occurred due to cracking perpendicular to the sample surface. Cracking all the way to the base metal may explain the hydrogen uptake, but it is clearly limited and localized at 1100 °C. Similar to early-time results observed after oxidation at 1000 °C, white spots of presumed monoclinic oxide appeared in a matrix of black tetragonal oxide (see Fig. 10a). After 512 s and 1400 s in steam at 1100 °C, white–grey areas were clearly visible (Fig. 10b and c, respectively). However, unlike the 1000 °C results for this hold-time range, the spots remained essentially isolated and were more stable in the black matrix. After ≈2500 s in steam at 1100 °C, the white spots grew, cracked and partially connected on the surface of the sample, and the oxide nodules grew deeply into the metal (Fig. 11). After 3800 s, more extensive cracking and inter-connection occurred (Fig. 10d). However, the hydrogen content was only ≈200 wppm at this exposure time, even though the appearance of the surface would suggest otherwise. This result indicates that some hydrogen was lost due to diffusion to the inner-surface, desorption to the argon purge, and transport by the purge for the one-sided oxidation performed at 1100 °C.

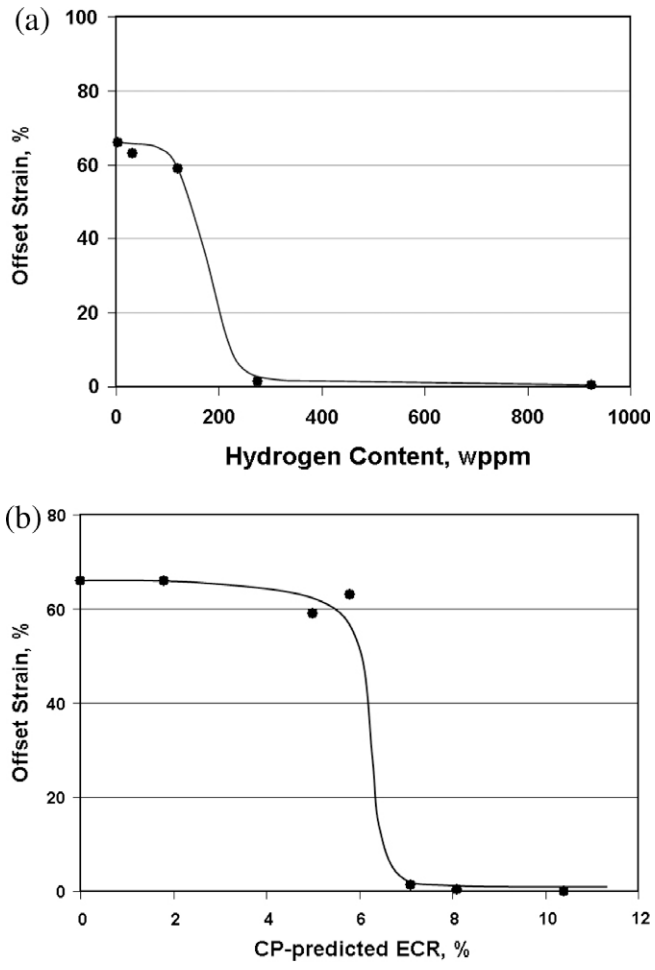

Fig. 9. Ductility results for as-received E110 tubing after two-sided oxidation tests at 1000 °C: (a) room-temperature (RT) offset strain vs. hydrogen content and (b) RT offset strain vs. CP-predicted ECR.

3.4. Testing of polished-only and machined-and-polished E110 samples

The high surface roughness/defects of as-received E110 (see Fig. 2a–d), as well as the surface/substrate chemistry, may contribute to the early formation of monoclinic oxide followed by local (1100 °C) and/or global (1000 °C) breakaway oxidation. Thus, steam-oxidation experiments were performed with M–P and polished-only samples. The results were encouraging in that breakaway oxidation was delayed for samples with polished and M–P surfaces. Additional tests were then performed to determine the weight-gain kinetics of E110 for periods during which the oxide layer remained lustrous black and intact. At 1000 °C, these times were extended to determine the hydrogen concentration vs. time and ECR. Tests were also conducted at 1100 °C and 1200 °C to determine ductility decrease with increasing hold time and oxidation level.

3.4.1. Two-sided oxidation at 1000 °C

In Test EU#13 (1000 °C for 290 s to 5% ECR), half of the sample was in the as-received condition, and half the sample was machined on the outer-surface (38 μm removed) and polished. Based on visual and low-magnification inspection (Fig. 12a), the oxide on the M–P segment appeared uniform and lustrous black, while the non-treated segment showed the mixture of white regions in a matrix of black oxide observed in the other tests with as-received E110. Metallography was performed to confirm that the black oxide layer on the M–P sample was intact (Fig. 12b), while the oxide on the as-received part of the sample was cracked and partially delaminated (Fig. 12c).

Test EU#14 was run to determine the relative benefits of polishing vs. machining and polishing on the steam-oxidation performance of E110 at 1000 °C and 290-s hold time. The sample consisted of three axial regions: machined (25 μm removed) and polished, polished only, and as-received. Fig. 13 shows that both the polished-only and the M–P sample preparations resulted in formation of a smooth, black oxide on the outer-surface, in contrast to the behavior of the as-received region. The low-magnification photograph in Fig. 13a suggests that polishing (see Section 2 for

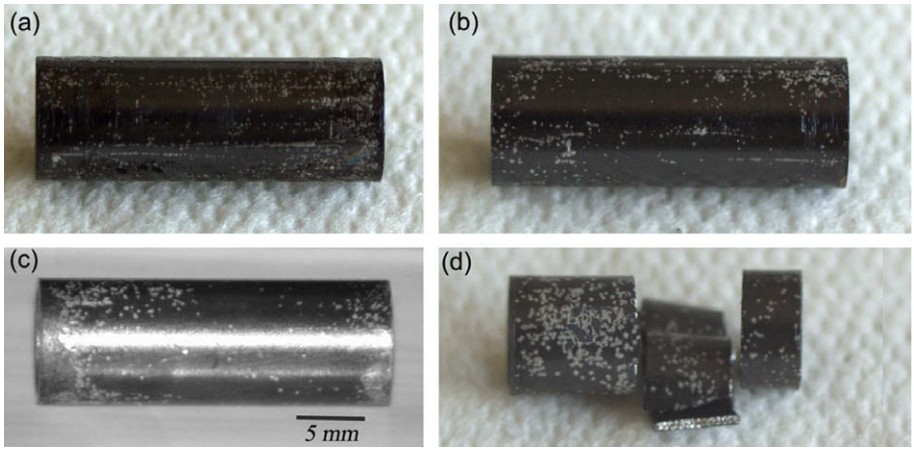

Fig. 10. Appearance of as-received E110 tubing outer-surface after steam-oxidation at 1100 °C for (a) 100 s, (b) 512 s, (c) 1400 s, and (d) 3800 s. The 3800 s sample shown in (d) was sectioned for ring compression testing and hydrogen analysis before the photograph was taken.

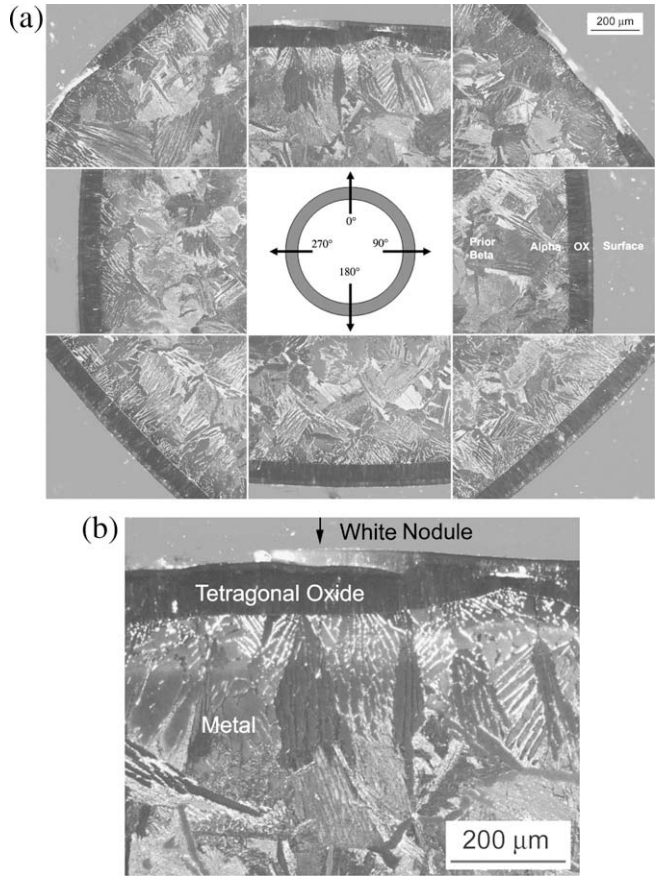

Fig. 11. (a) Circumferential variation of as-received E110 tubing microstructure after 2473 s of one-sided oxidation at 1100 °C, which shows flat interfaces between oxide and metal layers for five of the eight locations, and (b) higher magnification cross-sectional image, indicating growth of white monoclinic oxide nodes on top of black tetragonal oxide layers.

polishing procedure) alone is sufficient to improve the behavior of E110. Polishing smoothes out the surface roughness by removing a few microns from the surface. In the process, chemical impurities (i.e., trace elements) and alloy constituents near the surface are also removed. Higher (≈200×) magnification photographs show that the M–P outer-surface after oxidation has very small (≈25 μm), isolated spots of monoclinic oxide (see Fig. 13b). Larger regions of monoclinic (light-colored) oxide were observed for the polished outer-surface (Fig. 13c), and even larger regions were observed for the as-received material (Fig. 13d).

Clearly, the quality of the oxide layer on the polished surface is much better than that on the as-received surface. This finding suggests that the oxidation behavior of the E110 alloy is sensitive to some combination of surface roughness and surface chemistry. The performance was improved somewhat by the combination of the removal of 25 μm from the outer-surface and polishing of the machined surface. Thus, further improvement may be achieved by removing some of the near-surface layer, as well as the surface itself. Note that the untreated inner-surface of the sample exhibited large regions of monoclinic oxide visible at low magnification. However, neither treatment eliminated the initiation of monoclinic oxide spots, although both treatments slowed down the initiation and growth of the monoclinic regions and may have decreased significantly the number density of initiation sites. Also note that our experiments were conducted on as-received tubing materials. However, Yegorova et al. [14] observed the same early breakaway oxidation for finished cladding (pickled and anodized) and for irradiated cladding with thin (≈5 μm) corrosion-layer thickness.

Test EU#16 was run to determine if outer and inner-surface polishing would be sufficient to achieve ≈10% calculated ECR at 1000 °C without breakaway oxidation. As shown in Fig. 14, extensive formation of monoclinic oxide is evident on one side of the sample. Spallation and delamination of this oxide occurred during the cooling phase of the test. The remaining oxide surface underneath this spalled region is dull black and rough. The surfaces of other cladding alloys (e.g., M5) also have this appearance after classical breakaway oxidation at much longer times. However, about half the outer-surface still consists of lustrous-black oxide, which underwent no apparent delamination or spallation. High magnification images of this region show no evidence of monoclinic oxide formation. This behavior is in dramatic contrast to that of the as-received cladding (Fig. 6) under similar test conditions. However, further investigations are needed to understand the difference. Such behavior may result from the circumferential temperature variation if E110 breakaway oxidation is highly temperature sensitive.

The sample for Test EU#17 was machined and polished on the inner (20-μm removal) and outer (44-μm removal) surfaces and tested at the same temperature as the polished-only EU#16 sample, but for a longer time (1325 s vs. 1025 s at 1000 °C). The extent of monoclinic oxide formation, cracking, and spallation was as significant as for the EU#16 sample. As the oxidation furnace has a viewing window port, we were able to make several interesting

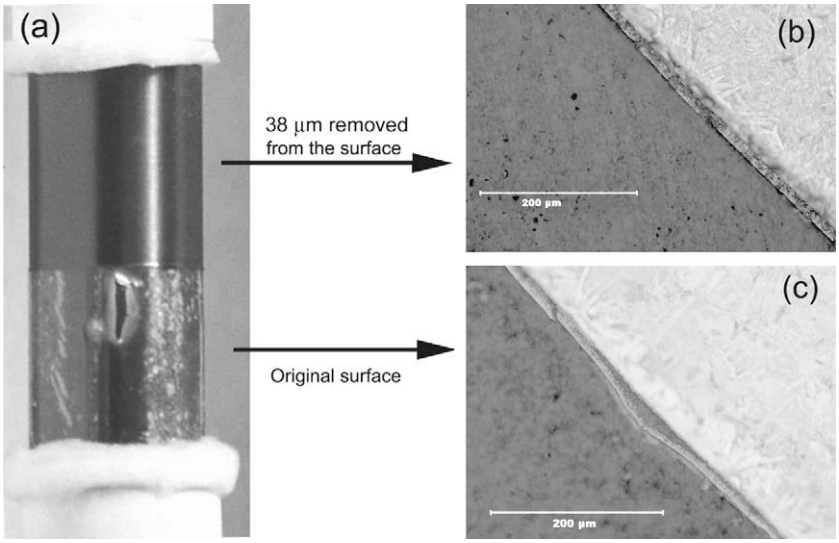

Fig. 12. (a) Machined-and-polished E110 outer-surface next to as-received E110 after steam-oxidation at 1000 °C for 290 s. Metallographic images show (b) intact oxide layer on machined-and-polished E110 surface and (c) cracked/delaminated oxide layer on as-received E110 surface.

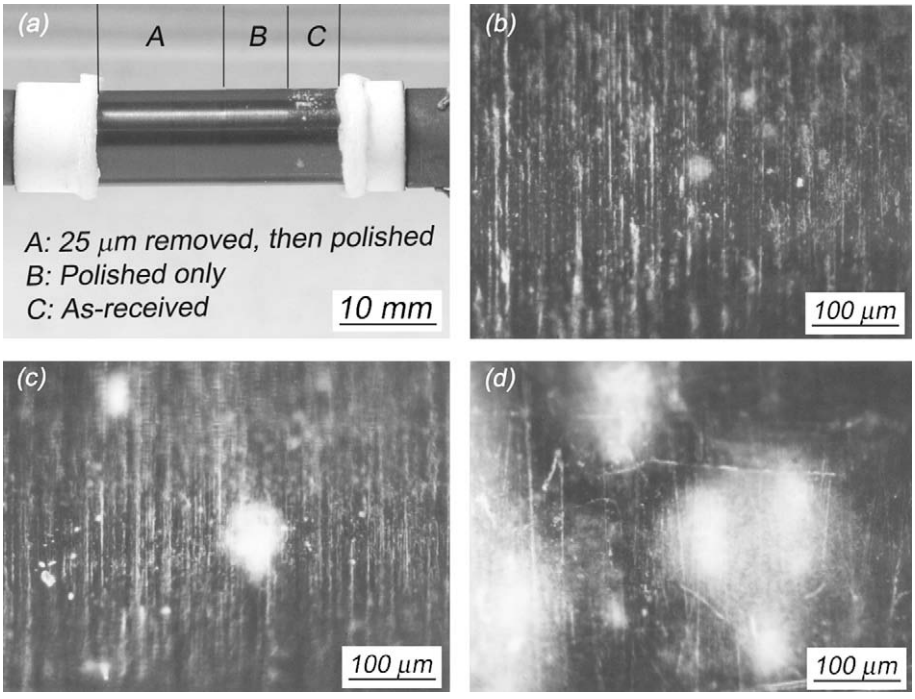

Fig. 13. (a) E110 sample after steam-oxidation at 1000 °C for 290 s (Test EU#14). High-magnification images show different areas in (a): (b) machined-and-polished E110, (c) polished E110, and (d) as-received E110.

observations about the outer-surface: (a) at 325 s into the hold time at 1000 °C, white spots appeared on the surface; (b) the surface oxide looked good from 325 to <1100 s; (c) breakaway oxidation initiated at ≈1100 s; and (d) extensive breakaway oxidation was evident at 1175 s. These observations may indicate that the breakaway oxidation time is highly sensitive to temperature in this regime. To better understand the differences between E110 and other cladding alloys during steam-oxidation, it is necessary to test these materials under the same conditions. For example, E110 has a thicker wall (0.71 mm) than the 17 × 17 M5 cladding (0.61 mm) tested at ANL, and its thermal response is slower in our test apparatus during the temperature ramp from 300 to 1000 °C. To ensure that the E110 and M5 samples experienced similar temperature histories, ≈115 μm was machined from the E110 inner-surface, and both the inner and outer-surfaces were polished. This treatment resulted in better agreement between the thermal masses and thermal responses of E110 and M5, as well as the wall thickness (≈0.61 mm) used to calculate ECR.

Results for the tests with modified E110 are listed in Table 4. The samples exhibited uniform black oxide layers at low magnification up to hold times of ≈240–290 s. The weight-gains (normalized to surface area) for samples that exhibited a uniform black oxide on the outer-surface are recorded in Table 4. These weight-gains at 1000 °C are less than those predicted by the CP model

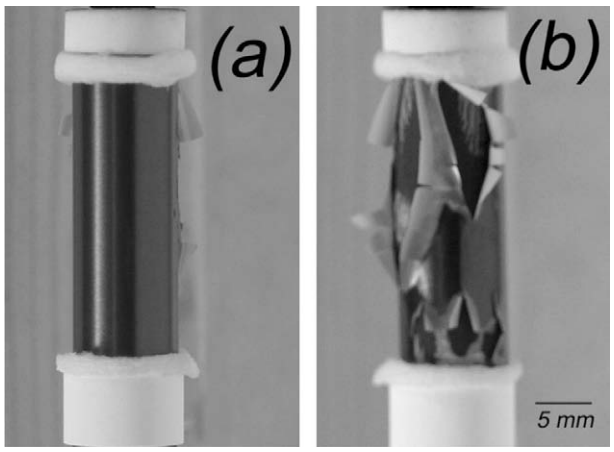

Fig. 14. Surface of polished E110 sample from Test EU#16 after 1025 s of two-sided oxidation in steam at 1000 °C. Extensive monoclinic oxide formation, delamination, and spallation are evident on one side of the sample (b), while the other side remains intact (a).

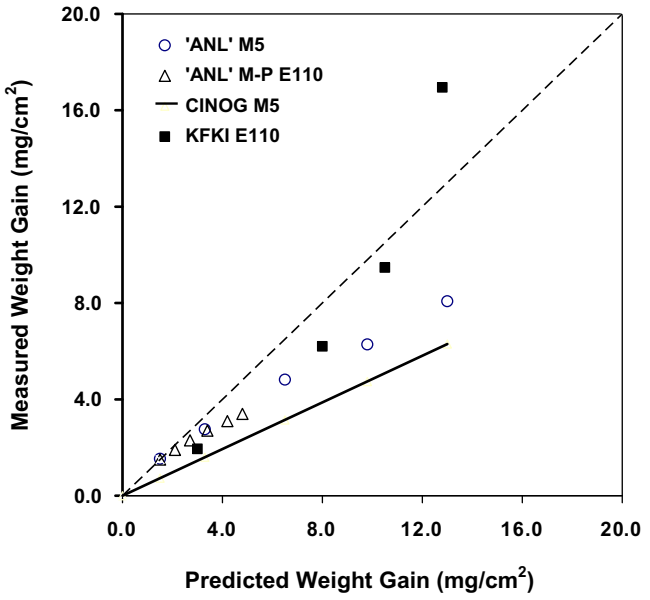

Fig. 15. Measured vs. predicted weight-gain from steam-oxidation at 1000 °C for machined-and-polished (M–P) E110 tested at ANL, as-fabricated M5 tested at ANL, E110 tested at KFKI [24], and M5 tested in the French CINOG experiments [25]. Predicted values for ANL tests (dashed line) are based on the integration of the CP weight-gain rate equation over the sample temperature profile.

(see Fig. 15). The weight-gain coefficient (k) at 1000 °C, for $\Delta w = k \cdot t^{0.5}$, is 0.2242 $(mg/cm^2)/s^{0.5}$ as determined by the CP model, compared with 0.162 $(mg/cm^2)/s^{0.5}$ measured for polished E110 (excluding data points for EU#22–23). Plotted in Fig. 15 are also the weight-gain results for M5 tested at ANL [18] and M5 tested in the CINOG experiments in France [25]. The derived k at 1000 °C for M5 tested at ANL is 0.135 $(mg/cm^2)/s^{0.5}$. As indicated in Fig. 15, the oxidation behavior of ANL M–P E110 is similar to that of M5 at 1000 °C for test times during which the E110 oxide layer remained intact (uniform and lustrous black). The measured weight-gain of KFKI [24] E110 increased faster with oxidation time than ANL E110 and M5. However, the KFKI data include E110 beyond the breakaway oxidation time based on both weight-gain increase and hydrogen pickup.

Additional tests were performed with polished and M–P E110 to determine the time at 1000 °C when the hydrogen content increased dramatically. This hydrogen increase correlates with the ductility decrease and the transition from ductile to brittle behavior. The test matrix and results for this series of tests are given in Table 4. The hydrogen content vs. CP-predicted ECR of the polished and M–P E110 is shown in Fig. 8, along with data for the as-received E110 tested at ANL and E110 tested at KFKI. Given the axial and circumferential variation of hydrogen content in these samples, some scatter was expected in the correlation between average hydrogen content for a ring and embrittlement. Also, the KFKI samples were only 8-mm long and were more susceptible to even earlier breakaway oxidation due to end effects than the ANL samples (25-mm long) and the Yegorova et al. [14] samples (100-mm long). Nonetheless, it is clear in Fig. 8 that the hydrogen pickup of the polished and M–P E110 is much slower than as-received E110 tested at both ANL and KFKI.

3.4.2. Steam-oxidation at 1100 °C

Experiments were conducted with machined (to ≈0.6-mm wall thickness) and polished E110 samples to determine the weight-gain kinetics at 1100 °C prior to breakaway oxidation, and the results were compared with those from other investigations [10,14]. Table 5 gives the test conditions and results. All samples exhibited a lustrous black oxide layer up to the highest test time (1011 s). At this test time, small white spots were observed on the outer-surface oxide layer. The weight-gain results for the ANL M–P E110 are plotted in Fig. 16 vs. the CP-predicted weight-gain, along with the Russian KI G110 [14] and KFKI E110 [24] data at 1100 °C. Unlike the results at 1000 °C, much better agreement is achieved between the E110 weight-gain kinetics and the CP-predicted values. Similar behavior was observed for M5 samples tested at Argonne. The weight-gain coefficient (k) at 1100 °C was determined to be 0.613 $(mg/cm^2)/s^{0.5}$ for the ANL M–P E110. The M–P samples oxidized at 1100 °C were subjected to RT ring-com-

Table 5
Comparison of E110 post-oxidation RT ductility between ANL machined-and-polished (M–P) cladding samples and Bochvar-TVEL (BT) lots 2–4 pickled cladding samples [27] Following two-sided steam-oxidation at 1100 °C. ECR is referenced to actual wall thickness.

E110 material	Wall thickness (mm)	Hold time (s)	CP ECR (%)	Measuerment ECR (%)	H content (wppm)	Offset displacement (mm)	Offset strain (%)	
ANL M–P	0.61	111	7.5	7.0	13	5.47	60	Lustrous black oxide
ANL M–P	0.69	361	10.5	9.2	13	2.86	31	Lustrous black oxide
BT lot 2	0.71	600	12	≈10	60–200	–	10	
BT lot 3	0.71	600	12	≈10	60–200	–	6.6	
BT lot 4	0.71	600	12	≈10	60–200	–	4.4	
ANL M–P	0.58	511	14.4	12.7	16	1.94	21	Lustrous black oxide
ANL M–P	–	576	–	–	–	–	–	Lustrous black oxide
ANL M–P	0.58	1011	19.4	16.0	20	0.58	6.3	Lustrous black oxide with small white spots

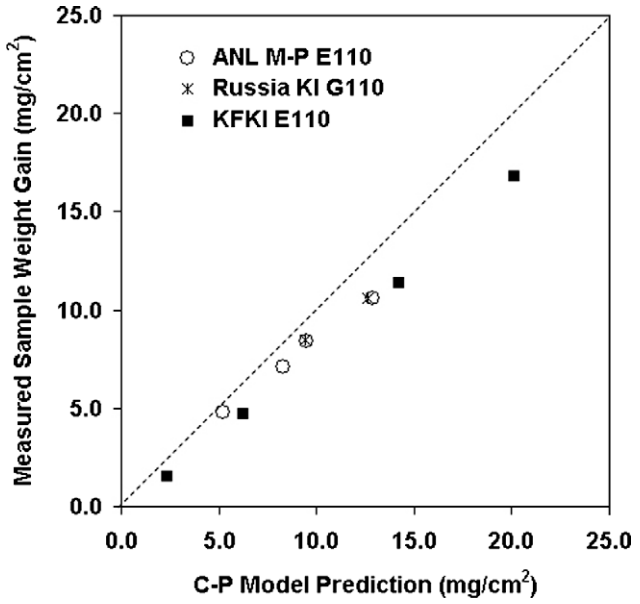

Fig. 16. Measured vs. predicted weight-gain for ANL machined-and-polished (M–P) E110 and Russian KI G110 [14] and KFKI E110 [24]. Solid line shows the CP model predictions for steam-oxidation at 1100 °C. Sponge Zr was used for the Zr-1Nb ingot from which G110 was fabricated.

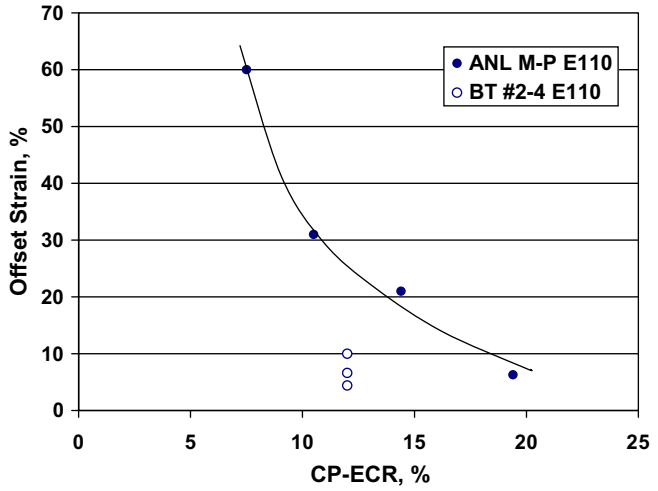

Fig. 17. Post-oxidation RT ductility vs. CP-ECR for ANL machined-and-polished (M–P) E110 and Bochvar-TVEL (BT) pickled E110 [27] following two-sided steam-oxidation at 1100 °C.

pression tests, the result of which are compared to the best of the Bochvar-TVEL results [27] in Table 5 and Fig. 17. The Bochvar-TVEL samples were characterized by low (25–45 wppm) trace elements (such as Ni, Al, Si, Ca, K, F, Cl, Na and Mg). However, Bochvar-TVEL E110 was pickled prior to testing. Pickling with an HF-containing acid results in additional surface-layer fluoride impurities. Although the weight-gain results from KFKI agree quite well with the ANL results at 1100 °C, the hydrogen pickup of the KFKI samples was much faster than that for the ANL samples, resulting in low embrittlement time $\geqslant$133 s [24]. From a comparison of the ANL and Bochvar-TVEL results, we concluded that polishing, which removes surface impurities, is more effective in delaying breakaway oxidation and hydrogen pickup than controlling trace elements in the bulk of the material.

3.4.3. Steam-oxidation at 1200 °C

Machined-and-polished E110 samples were oxidized at 1200 °C and quenched at 800 °C, which is more prototypical of "real" LOCA transients than furnace cooling. The ring-compression tests were conducted at 135 °C. Because the ductility of the ANL-modified E110 was so good following 1100 °C oxidation, the 1200 °C-oxidized samples were tested to see how they compared to the US alloys. Table 6 summarizes the results for oxidation levels and ring-compression offset strains for these E110 samples. All samples were lustrous black with negligible hydrogen pickup. For $\leqslant$13% CP-ECR, the ductility of ANL-modified E110 oxidized at 1200 °C is higher than that of as-received E110 [14], an older vintage (HBR-type) of 15 × 15 Zry-4, and modern 17 × 17 Zry-4 cladding. The post-oxidation ductility of ANL-modified E110 is comparable to that of 17 × 17 M5 at 13% CP-ECR, which was reported in Refs. [15,18]. The ductile-to-brittle transition CP-ECR for ANL-modified E110 oxidized at 1200 °C was not determined in this work. However, as-received E110 oxidized at 1200 °C experienced significant breakaway oxidation, hydrogen pickup, and embrittlement [14] as compared to polished E110 tubing tested at ANL.

4. Discussion

Breakaway oxidation has been investigated by Leistikow and Schanz [3,4] for an older vintage of standard Zry-4 (1.6 wt.% Sn, 0.12 wt.% O, and 0.725-mm wall thickness) and by Mardon et al. [16] for polished 17 × 17 low-tin Zry-4 (1.29 wt.% Sn, 0.12 wt.% O, and ≈0.1-μm surface roughness) and polished M5. Although the breakaway oxidation time is generally defined as the time corresponding to an increase in oxidation rate (i.e., weight-gain rate), we believe that the associated hydrogen pickup is a more appropriate metric for the determination of breakaway oxidation time. The increased hydrogen content, along with the increased oxygen content, in the prior-beta layer induces embrittlement. For oxidation temperatures $\leqslant$1000 °C, the cladding alloys tested at ANL remained ductile at 135 °C for hydrogen pickup <200 wppm. Thus, 200-wppm hydrogen pickup is used by ANL as the metric to determine the minimum breakaway oxidation time.

Leistikow and Schanz presented trend curves (see Fig. 6 in Ref. [4]) for weight-gain vs. time and temperature and a data plot (see Fig. 8 in Ref. [4]) for hydrogen content vs. time at 650–1000 °C. Their sample preparation included degreasing, pickling in a nitric–fluoric acid mixture, and cleaning in boiling water. Such treatment may leave a fine surface layer containing fluorine impurities.

Table 6
Post-oxidation ductility at 135 °C for ANL machined-and-polished E110 samples that were oxidized at 1200 °C and quenched at 800 °C (9.07-mm polished outer diameter, 7.87-mm machined-and-polished inner-surface, and 0.6-mm wall thickness). ECR is referenced to actual wall thickness.

E110 test #	Wall thickness (mm)	Test time[a] (s)	CP-ECR (%)	Measurement ECR (%)	Offset displacement (mm)	Offset strain (%)
EU#53	0.60	136	7.5	8.6	>5	>55
EU#51	0.60	192	10.0	10.4	>5	>55
EU#52	0.61	211	13.0	13.8	1.47	16
	0.61		13.0	13.8	0.66	7

[a] From ramp initiation at 300 °C to end of hold time at 1200 °C.

The combination of high surface roughness and surface fluorine impurities can destabilize the oxide layer growth through early transformation from the tight tetragonal phase to the weaker monoclinic phase. Two-sided oxidation tests were performed in their study. Thus, the condition of the cladding inner-surface may have influenced the breakaway oxidation times.

Mardon et al. [16] reported hydrogen-concentration results vs. time at 1000 °C for modern, polished 17 × 17 low-tin Zry-4. The oxidation was one-sided and on the outer-surface only. Thus, the condition of the cladding inner-surface (grit-polished vs. belt- or wheel-polished) had no influence on the results. It is clear that polished 17 × 17 low-tin Zry-4 has a much longer breakaway time (≈5400 s) at 1000 °C than the pickled-and-cleaned, rough-surfaced, older Zry-4 (≈1800 s).

Breakaway oxidation time is not a monotonic function of decreasing or increasing oxidation temperature. From the work of Leistikow and Schanz, minimum breakaway oxidation times for Zry-4 appear to occur at oxidation temperatures of 750–800 °C and 1000 °C. In terms of hydrogen pickup, oxidation at 1000 °C gives the minimum breakaway time. For most ANL tests, we concentrated on breakaway oxidation at 1000 °C – particularly the effects of surface conditions.

The classical view of the progression leading to breakaway oxidation for Zry-4 given by Leistikow and Schanz (LS) is:

(a) breakaway oxidation instability initiates at the metal-oxide interface with local formation of monoclinic oxide;
(b) the precursor to breakaway oxidation is the transition from a "flat" oxide-metal interface to a wavy interface (i.e., described as scalloped by LS);
(c) the wavy surface creates alternating regions of tensile and compressive stresses in the near-surface oxide;
(d) local regions under tensile stress transform first from tetragonal-to-monoclinic oxide;
(e) the tetragonal-to-monoclinic oxide transition spreads from the inner-surface to the outer-surface; and
(f) cracking of the weak monoclinic oxide increases the weight-gain rate and hydrogen pickup rate.

Applying this conceptual model to experimental results indicates that, by the time the outer-surface of Zry-4 samples is observed to turn from black to gray, the weight-gain rate and hydrogen-pickup rate are such that the oxide is well into the breakaway regime, and the minimum breakaway oxidation time is exceeded. Our study indicated that breakaway oxidation for modern Zry-2, Zry-4, ZIRLO and M5 [4,18] likely follows the LS model. However, that is not the case for E110.

For E110, our results reveal that "white spots", initiation sites for nodular oxidation, formed in the black matrix at a very early stage of steam-oxidation (75-s ramp and the 5-s hold time at 1000 °C), as shown in Figs. 6a and 7a. At ≈365 s (290-s hold time at 1000 °C), white spots developed into local regions of nodular oxidation, and then into interconnecting regions (see Fig. 6b). Extended breakaway oxidation and high hydrogen uptake (≈540 wppm) were observed after 975 s of oxidation, and then extreme breakaway oxidation and hydrogen uptake (≈4230 wppm) were evident after 1475 s of oxidation. This oxidation behavior is consistent with the results obtained for E110 by other investigators [14,19].

Metallographic examinations show a flat interface between the metal layer and oxide layer for the E110 sample oxidized for a 75-s ramp to 1000 °C and a 5-s hold time at 1000 °C, although the white spots had already initiated on the OD surfaces (Fig. 7b). Moreover, the flat interface between the metal layer and oxide layer is also observed (Fig. 11) after 2473 s of one-sided oxidation at 1100 °C, for which some interconnection of white spots is apparent on the surface. Although white nodules are clearly viewed on top of the black oxide layer in Fig. 11b, no wavy oxide/metal interface is observed in that area as well as all other areas (Fig. 11a). For all other alloys tested by ANL, a wavy (i.e., scalloped) oxide-metal interface always appeared prior to the breakaway time determined by hydrogen pickup. This finding implies that the unusual oxidation behavior of E110 around 1000 °C does not result from local tensile stresses developed at the metal-oxide interface after long-time oxidation, as suggested by the LS model. Rather, we believe that E110 breakaway is due to chemical impurities in the oxide layer causing the transformation, for which surface impurities and substrate impurities appear to drive the ZrO_{2-x} to ZrO_2. The stresses due to abrupt changes in geometry from sample ends, surface roughness, and scratches appear to enhance the breakaway process in E110. However, they are not sufficient to induce the breakaway without the presence of chemical impurities. The older-vintage Zry-4 tubing tested at ANL had a comparable surface roughness (0.35 μm) and the same end effects. However, breakaway did not occur until 3800 s at ≈1000 °C after the development of a scalloped metal-oxide interface, and it did not occur at the ends of the sample. Although polishing E110, which both removes surface impurities and decreases surface roughness, delayed E110 breakaway oxidation, the cause of the improved behavior appeared to be more due to the removal of surface impurities rather than the decrease in surface roughness.

Our studies have indicated that machining and polishing can further delay the breakaway time to about 1100 s (75-s ramp and 1100-s hold time at 1000 °C) for E110, but that time is still much shorter than the 6000 s at 1000 °C for M5 [16], even though both alloys have similar composition. Therefore, the oxidation behavior of the Zr-1Nb alloys at elevated temperatures is sensitive not only to alloy composition but also to impurities (trace elements). A mixture of iodide and electrolytic Zr is used for the fabrication of the typical E110 alloy [14], whereas sponge Zr is used for the fabrication of western alloys such as Zry-4, M5, and ZIRLO. Clearly, the different processes can result in different impurity compositions, as a result of which the oxidation behavior could be changed. This observation is confirmed by the modified types of E110 fabricated from sponge Zr by the Russian industry (referred to as G110 or $E110_{G(fr)}$ in Ref. [14]). For oxidation at 900–1000 °C, the sponge E110 oxidation and hydrogen pickup were reduced significantly in comparison with those of the iodide/electrolytic E110 [14]. Accordingly, the minimum breakaway time for sponge E110 also increased, the details of which are given in Ref. [14]. For E110 fabricated from sponge Zr, only minimal breakaway oxidation and hydrogen pickup were observed after 5000 s at 1000 °C.

Our microstructural examinations show mainly two SPP types in E110: Nb-rich precipitates (see Figs. 4b and 5b) and precipitates containing less Nb but some Fe (Figs. 4b and 5c). Although only beta-phase SPP enriched with Nb were reported by Shishov et al. [26] and Yegorova et al. [14] in E110 alloy, these two precipitates were observed by Mardon et al. in M5 [10], for which the breakaway time was reported to be about 6000 s. However, a high density of precipitates was observed in a local area of as-received E110 (Fig. 4c), which was not reported before for either E110 or M5 alloys. As this was observed in a very small region, more characterization is needed to confirm whether the clusters of precipitates exist globally in E110 and whether they contribute to early breakaway oxidation.

The effects of impurities on nodular oxidation of Zr-based alloys were discussed by Chung [28] with regard to charge balance, oxygen ion vacancy, stoichiometry, crystal structure and fracture toughness of Zr oxide phases. Fluorine pickup, related to fabrication processes of some alloys (such as E110), is believed to be detrimental because it leads to increased susceptibility to nodular oxidation. On the other hand, pickup of undervalent impurities

(Ca, Mg and Al) during Hf purification and the production of sponge Zr may be beneficial because they help maintain the hypostoichiometry [$ZrO_{(2-x)}$] needed to stabilize the tetragonal phase.

The progression leading to breakaway oxidation for E110 can be summarized as follows:

(a) nodular oxidation initiates at chemical impurity sites in the oxide layer (or near the interface between the oxide and metal layers) with local formation of monoclinic oxide;
(b) the nodules spread in radial, circumferential, and axial directions;
(c) hydrogen pickup starts locally when the nodules reach the metal throughout the oxide layer thickness; and
(d) the nodules connect to each other and eventually cause extensive breakaway of the oxide layer.

5. Conclusions

Steam-oxidation tests were conducted with samples from E110 tubing at temperatures of 1000–1200 °C for the purpose of examining the behavior of this alloy under postulated LOCA conditions in LWRs. The following conclusions were made from the results:

(1) The E110 tubing tested at Argonne showed a high susceptibility to nodular oxidation and breakaway oxidation at relatively low test times in steam at 1000–1100 °C, as compared to other alloys tested under the same conditions. At 1000 °C, the nodules grew rapidly along the E110 surface, interconnected, cracked, delaminated, and spalled at relatively low test times. At 1100 °C, the nodules grew into the E110 wall (oxygen-stabilized alpha layer) with relatively slow growth along the surface.
(2) During the transition from initiation of breakaway oxidation to extensive delamination and spallation, the hydrogen content showed significant variation in the circumferential and axial directions: the concentration was high under regions of cracked "white" oxide and low under regions of intact "black" oxide. The growth rate, along with the associated hydrogen uptake, was enhanced by partial and through-thickness cracking of the nodules. The hydrogen uptake was >100 wppm after a hold time of ≈300 s and >500 wppm after a hold time of ≈600 s at 1000 °C.
(3) The breakaway time for the E110 tested in the ANL program was increased significantly by polishing only or by machining and polishing the tubing surfaces. For polished samples oxidized in steam at 1100 °C, no significant nodular oxidation was observed up to a hold time of ≈1000 s. For polished samples oxidized in steam at 1000 °C, a lustrous black oxide was maintained up to ≈400 s, and hydrogen uptake >100 wppm was delayed until >900 s. The improved behavior is attributed primarily to the removal of surface and substrate impurities (e.g., fluorine) and, secondarily, to the decrease in roughness and surface scratches, which cause local stress concentrations.
(4) For the ANL M–P tubing, the weight-gain coefficients under pre-breakaway oxidation conditions were:
$k_{1000} = 0.162\ (mg/cm^2)/s^{0.5}$ for $T = 1000$ °C
$k_{1100} = 0.613\ (mg/cm^2)/s^{0.5}$ for $T = 1100$ °C.

Acknowledgments

This work was sponsored by the Office of Nuclear Regulatory Research, US Nuclear Regulatory Commission (NRC). The electron microscopy was performed at the Electron Microscopy Center at Argonne National Laboratory, a US Department of Energy Office of Science Laboratory operated under Contract No. DE-AC02-06CH11357 by UChicago Argonne, LLC. We would like to express our appreciation to R. Cook and J. Hiller for their help on SEM and TEM examinations. We are indebted to R. Terasvirta of Fortum for proving us with E110 tubing and cladding. We are particularly grateful to H.H. Scott (NRC) for managing this program and to R.O. Meyer (NRC) for his technical guidance in pre-test planning and post-test data interpretation, which resulted in significant contributions to this work.

References

[1] L. Baker, L.C. Just, Studies of Metal-Water Reactions at High Temperatures: III. Experimental and Theoretical Studies of the Zirconium-Water Reaction, ANL-6548, May 1962.
[2] J.V. Cathcart, R.E. Pawel, R.A. McKee, R.E. Druschel, G.J. Yurek, J.J. Campbell, S.H. Jury, Zirconium Metal-Water Oxidation Kinetics: IV. Reaction Rate Studies, ORNL/NUREG-17, August 1977.
[3] S. Leistikow, G. Schanz, Werkstoffe und Korrosion 36 (1985) 105.
[4] S. Leistikow, G. Schanz, Nucl. Eng. Des. 103 (1987) 65.
[5] H.M. Chung, T.F. Kassner, J. Nucl. Mater. 84 (1979) 327.
[6] Y. Yan, R.V. Strain, T.S. Bray, M.C. Billone, High Temperature Oxidation of Irradiated Limerick BWR Cladding, NUREG/CP-0176, May 2002, pp. 353–372.
[7] G. Hache, H.M. Chung, The History of LOCA Embrittlement Criteria, NUREG/CP-0172, May 2001, pp. 205–237.
[8] S. Kawasaki, T. Furyta, M. Suzuki, Nucl. Sci. Tech. 15 (1978) 589.
[9] F. Nagase, T. Otomo, H. Uetsuka, Nucl. Sci. Tech. 40 (2003) 213.
[10] J.-P. Mardon, D. Charquet, J. Senevat, Influence of composition and fabrication process on out-of-pile and in-pile properties of M5 alloy, in: G.P. Sabol, G.D. Moan (Eds.), Zirconium in the Nuclear Industry: 12th International Symposium, ASTM STP 1354, American Society for Testing and Materials, West Conshohocken, PA, 2000, pp. 505–524.
[11] R.J. Comstock, G. Schoenberger, G.P. Sabol, Influence of processing variables and alloy chemistry on the corrosion behavior of ZIRLO nuclear fuel cladding, in: E.R. Bradley, G.P. Sabol (Eds.), Zirconium in the Nuclear Industry: 11th International Symposium, ASTM STP 1295, American Society for Testing and Materials, 1996, pp. 710–725.
[12] P.V. Shebaldov, M.M. Peregud, A.V. Nikulina, Y.K. Bibilashvilli, A.F. Lositski, N.V. Kuz'menko, V.I. Belov, A.E. Novoselov, E1110 alloy cladding tube properties and their interrelation with alloy structure-phase condition and impurity content, in: G.P. Sabol, G.D. Moan (Eds.), Zirconium in the Nuclear Industry: 12th International Symposium, ASTM STP 1354, American Society for Testing and Materials, West Conshohocken, PA, 2000, pp. 545–559.
[13] W.J. Leech, Ductility Testing of Zircaloy-4 and ZIRLO™ Cladding after High Temperature Oxidation in Steam, NEA/CSNI/R(2001)18, OECD Nuclear Agency, December 2001, pp. 135–143.
[14] L. Yegorova, K. Lioutov, N. Jouravkova, A. Konobeev, V. Smirnov, V. Chesanov, A. Goryachev, Experimental Study of Embrittlement of Zr-1%Nb VVER Cladding under LOCA-Relevant Conditions, NUREG/IA-0211, March 2005.
[15] Y. Yan, T. Burtseva, M.C. Billone, LOCA Results for Advanced-Alloy and High-Burnup Zircaloy Cladding, NUREG/CP-0185, June 2004, pp. 97–121.
[16] J.P. Mardon, J.C. Brachet, L. Portier, V. Maillot, T. Forgeron, A. Lesbros, N. Waeckel, Influence of Hydrogen Simulating Burn-Up Effects on the Metallurgical and Thermal-Mechanical Behavior of M5™ and Zircaloy-4 Alloys under LOCA Conditions, ICONE13-50457, in: 13th Intl. Conf. on Nucl. Eng., Beijing, China, May 16–20, 2005, pp. 1–9.
[17] J.C. Brachet, L. Portier, J. Hivroz, D. Hamon, T. Guilbert, T. Bedel, P. Yvon, J.P. Mardon, P. Jacques, Influence of Hydrogen Content on the α/β Phase Transformation Temperature and on the Thermal-Mechanical Behavior of Zy-4, M4 (ZrSnFeV), and M5™ (ZrNbO) Alloys During the First Phase of LOCA Transient, in: G.D. Moan, P. Rudling (Eds.), Zirconium in the Nuclear Industry, ASTM STP 1423, American Society for Testing and Materials, 2002, pp. 673–701.
[18] M. Billone, Y. Yan, T. Burtseva, R. Daum, Cladding Embrittlement During Postulated Loss-of-Coolant Accidents, NUREG/CR-6967, ANL-07/04, July 2008.
[19] J. Boehmert, M. Dietrich, J. Linek, Comparative studies on high-temperature corrosion of Zr-1%Nb and zircaloy-4, Nucl. Eng. Des., 147(1) (1993).
[20] J.H. Baek, K.B. Park, Y.H. Jeong, J. Nucl. Mater. 335 (2004) 443.
[21] F. Nagase, T. Fuketa, Nucl. Sci. Tech. 42 (2005) 209.
[22] L. Portier, T. Bredel, J.C. Brachet, V. Maillot, J.P. Mardon, A. Lesbros, Influence of long service exposures on the thermal-mechanical behavior of Zy-4 and M5™ alloys in LOCA conditions, J. ASTM Intl., 2(2) Paper JAI12468 (2005).
[23] J.-C. Brachet, V. Vandenberghe-Maillot, L. Portier, D. Gilbon, A. Lesbros, N. Waeckel, J.-P. Mardon, Hydrogen content, preoxidation, and cooling scenario effects on post-quench microstructure and mechanical properties of zircaloy-4 and M5® alloys in LOCA conditions, J. ASTM Intl., 5(5) (2008). Available online as JAI101116 at <www.astm.org>.
[24] Z. Hozer, C. Gyori, L. Matus, M. Horvath, J. Nucl. Mater. 373 (2008) 415.

[25] A. Le Bourhis, Justification of the M5™ Behavior in LOCA, in: Proc. Topical Meeting on LOCA Fuel Safety Criteria, NEA/CSNI/R(2001) 18, OECD Nuclear Agency, 2001, pp. 105–133.
[26] V.N. Shishov, A.V. Nikulina, V.A. Markelov, M.M. Peregud, A.V. Kozlov, S.A. Averin, S.A. Kolbenkov, A.Ye. Novoselov, Influence of Neutron Irradiation on Dislocation Structure and Phase Composition of Zr-Base Alloys, in: 11th International Symposium on Zirconium in the Nuclear Industry, Garmish-Parten-Kirhen, Germany, September 11–14 1995, ASTM STP 1295, American Society for Testing and Materials, 1996, pp. 603–621.
[27] V. Nikulina, L.N. Andreeva-Andrievskaya, V.N. Shishov, Yu.V. Pimenov, Influence of Chemical Composition of Nb Containing Zr Alloy Cladding Tubes on Embrittlement under Conditions Simulating Design Basis LOCA, in: Presentation at the 14th Intl. Symp. on Zirconium in the Nuclear Industry, Stockholm, Sweden, June 13–17, 2004, available upon request.
[28] H.M. Chung, The Effects of Aliovalent Elements on Nodular Corrosion, in: Proc. 2003 Nuclear Safety Research Conference, NUREG/CP-0185, 2004, pp. 283–298.